Light Scattering Data Evaluation using Legendre Polynomials

Diethelm Fröse

Carl Gustav Carus-Institut, Am Eichhof, D-75223 Niefern-Öschelbronn, Germany

Summary

Calculation of the masses and the radii of gyration from static light scattering experiments were performed by approximating the measured angle distributions by Legendre polynomials. The method allows a very good fit to the scattering angle 0°. In this paper the method is discussed applied to discretised theoretical form factors of several geometries as well as measured data of latex particles.

If the sample is polydisperse, the resulting form factor is the sum of the form factors of the individual particles. An iterative method was developed, that allows the deconvolution of form factors of spherical particles from the measured form factor to give information about the polydispersity of the sample. This form factor analysis will be discussed for experiments using asymmetrical Flow-Field-Flow-Fractionation (a-FFFF) of complex plant extracts to interpret the measured form factor as the superimposition of two possible elution modes of the a-FFF.

Approximation of Scattering Form Factors by Legendre - Polynomials

The angular dependence of the scattering intensity for static light scattering experiments can be expressed for particles at low concentration as [1]

$$\frac{R(\vartheta)}{Kc} = M\,P(\vartheta) \qquad (1)$$

where $R(\vartheta) := \frac{I}{I_0} r^2$ is the Rayleigh Ratio with the normalized scattering intensity I/I_0 times the the square of distance r from the scatterer center to detector; $K := \frac{(2\pi\, dn/dc\, n)^2}{N_a \lambda^4}$ the contrast factor with n = refractive index, dn/dc = refractive index increament, N_A = Avogardo number, λ = wavelength of the incident light in vacuum, M and c are molar mass and concentration of the dissolved component. $P(\vartheta)$ is the form factor, which describes the angular scattering behaviour of the particle. Taking into account, that the particles in dilute solution can adopt all possible orientations, the form factor can be developed into a taylor expansion. The result is the Zimm-approximation [2,3]:

$$\frac{R(\vartheta)}{Kc} = M\left(1 - \tfrac{1}{3}\left\langle r_g^2 \right\rangle \left(\frac{4\pi}{\lambda}\right)^2 \sin^2 \tfrac{\vartheta}{2} \pm \ldots\right) \qquad (2)$$

 CCC 1022-1360/00/$ 17.50+.50/0

with the radius of gyration $r_g=\langle r_g^2\rangle^{1/2}$. The angle brackets indicate the average over all possible conformations.

$$\left\langle r_g^{\,2}\right\rangle := \int_{all\,r}\rho(r)\,r^2\,dr \qquad (3)$$

The radius of gyration of the particle can be calculated from the initial slope by extrapolation of the measured *R/Kc*, plotted against $\sin^2 \vartheta/2$; the intercept of the curve extrapolated towards $\sin^2 \vartheta/2=0$ is M_w, the weight-average molar mass.

The correct fit is often a serious problem because of the discrete number of scattering angles and the strong curvature of the angular dependence for large particles. The task is to find a function, that fits the measured data and allows reliable extrapolation to zero angle. Mostly the Zimm plot is used where the reciprocal scattering intensity *Kc/R(ϑ)* is plotted against $\sin^2 \vartheta/2$, or more general, against $q^2=\left(4\pi n_0/\lambda \sin \vartheta/2\right)^2$. The strongly curved *P(ϑ)* often becomes largely linearized and can then be safely extrapolated to q=0. In case of weak curvature a simple polynomial fit serves satisfactorly. For pronounced curvature serious errors can still be introduced and several other techniques have to be applied. Most common are the Berry plot or the Guinier plot for the inverse scattering intensities.

In this work a further method is suggested. The measured data are fitted by a series of transformed Legendre polynomials. Legendre polynomials are orthogonal functions, where the members are [4]

$$\begin{aligned} P_0(x) &= 1 \\ P_1(x) &= x \\ P_2(x) &= \tfrac{1}{2}(3x^2-1) \\ &\vdots \\ P_{n+1}(x) &= \frac{1}{n+1}\left((2n+1)xP_n(x)-nP_{n-1}(x)\right) \end{aligned} \qquad (4)$$

These functions are defined in the range of $x\in[-1,1]$, while in experiments the range from $s\in[0,1]$ is covered. Defining a new variable $s:=(1-x)/2$, the range of the functions is transformed into the required interval of $s\in[0,1]$ and the functions *P(s)* become

$$
\begin{aligned}
P_0(s) &= 1 \\
P_1(s) &= 1-2s \\
P_3(s) &= 1-6s+6s^2 \qquad (5)\\
&\vdots \\
P_{n+1}(s) &= \frac{1}{n+1}\left((2n+1)(1-2s)P_n(s)-nP_{n-1}(s)\right)
\end{aligned}
$$

The measured form factor $P(\vartheta)$ can now be developed in a series of these transformed Legendre polynomials $\tilde{P}(s)$ with $s := \sin^2 \vartheta/2$

$$\tilde{P}(\sin^2 \vartheta/2) = \sum_{i=0}^{\infty} a_i P_i\left(\sin^2 \vartheta/2\right) \qquad (6)$$

where the a_i are the coefficients to be found. The advantage of the Legendre polynomials is their orthogonal behaviour, which permits *calculation* of these coefficients from the measured scattering intensities according to the relationship

$$a_i = \frac{2i+1}{2}\int_0^1 P(\sin^2 \vartheta/2) P_i\left(\sin^2 \vartheta/2\right) d(\sin^2 \vartheta/2) \qquad (7)$$

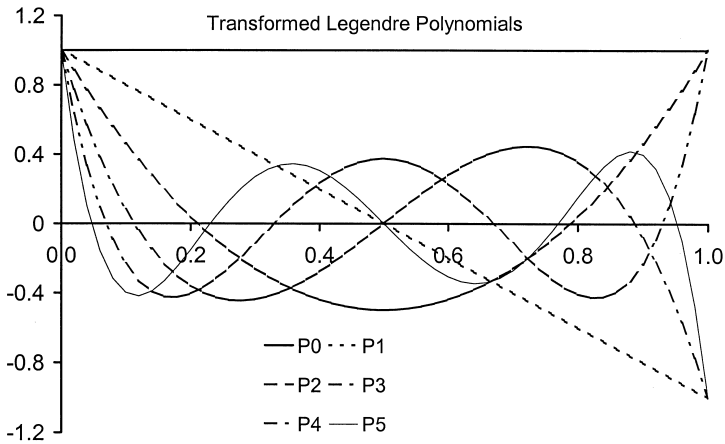

Figure 1: Plots of the first 6 transformed Legendre polynomials *P(s)*. These functions are well suited for development of the form factor, because the negative slope for small s values is very high even for a low polynomial degree.

The integration determining the a_i has to be performed over the range $\vartheta = 0$ to π; but the measured form factor $P(\sin^2 \vartheta/2)$ is known for only a discrete number of angles. In a first

approximation the unknown range was calculated by linear extrapolation between the two nearest data points. For the estimation of the first interval the linear interpolation between the first two known values was used extended to this interval. This leads to a certain error, that probably is small and will be discussed later.

An important point is the trunctation of the power series. If the data are noisy, the higher terms would be strongly influenced by the experimental error. In this work a criterion was used, that three succeeding coefficients have to be smaller than a fixed value (=0.03) or if one coefficient becomes smaller than zero. The latter is a neccessary condition to avoid a positive slope for $\vartheta=0$, that would be meaningless.

Treatment of Polydispersity

Using the Legendre formalism, an analytical expression for the form factor can be obtained according to eq. (6). If the sample is polydisperse, the form factor is the avarage over all form factors of the particles in the measuring cell, indicated by the radius r:

$$P_{poly}(\sin^2 \vartheta/2) = \int_0^\infty \alpha'(r) P(r, \sin^2 \vartheta/2) dr \quad (8)$$

The resulting mean square radius of gyration is the z-average over all particles $\langle r_g^2 \rangle_z$, the mass the weight-average M_w. To obtain more information on the system than only these avarage data, a deconvolution of form factors from spheres was performed. The following treatment is outlined with the examples of hollow spheres, whose form factor is especially simple known to be $P(q) = \left(\frac{\sin qr}{qr} \right)^2$ [5] with r the sphere radius and $q = \frac{4\pi n_0}{\lambda} \sin \vartheta/2$. The form factor of an ensemble of different sized particles can then be expressed by the following integral:

$$P_{poly}(\sin^2 \vartheta/2) = \int_0^\infty \alpha'(r) \left(\frac{\sin qr}{qr} \right)^2 dr \quad (9)$$

The function $\alpha'(r)$ represents a distribution function for the different sizes. The deconvolution was approximated using an iterative method. Expression (9) was approximated by N form factors of different size, the function $\alpha'(r)$ became then an N-dimensional vector $\vec{\alpha}$, where every component α_i means the moiety of the sphere with the radius r_i to the form factor.

Likelywise the form factor $P_{poly}(\sin^2 \vartheta/2)$ was represented by an M-dimensional vector $\vec{P}_{poly}$ corresponding to the M measured angles. The result is a system of M×N equations:

$$P_{poly,j}(\vec{\alpha}) = \sum_{i=1}^{N} \alpha_i \left[\frac{\sin\left(\frac{4\pi r_i}{\lambda} \sin \vartheta_j/2\right)}{\frac{4\pi r_i}{\lambda} \sin \vartheta_j/2} \right]^2 \quad (10)$$

A mathematically exact inversion of eq. (10) is not possible for functions which are superimposed by experimental errors; mathematecally the problem is ill – posed. Quite different distributions $\vec{\alpha}(r)$ can result into very similar form factors $\vec{P}_{poly}$. Therefore, an iterative method was used. Starting with an estimated distribution vector $\vec{\alpha}^0(r)$ (for instance $\vec{\alpha}^0(r) = \vec{1}$) the corresponding form factor $\vec{P}^0{}_{poly}$ was calculated using eq. (10). With the difference to the experimental values a mean square deviation $\Delta(\vec{\alpha}(r))$ was determined

$$\Delta(\vec{\alpha}) = \sum_{j=1}^{M} \left(P_{exp,j} - P_{poly,j}(\vec{\alpha})\right)^2 \quad (11)$$

In order to find a minimum for this deviation, the following methode was used. In general, the gradient of a function $f: \mathbb{R}^n \rightarrow \mathbb{R}$, which means the change $\frac{\partial f(x)}{\partial x_i}$ for a small change in every component x_i, points in the $\mathbb{R}^n$ - plane towards the direction of the increasing function. This property was used to calculate next value $\vec{a}^1(r)$. The gradient of the mean square deviation $\Delta(\vec{\alpha}(r))$ was calculated with $\vec{a}^n(r)$ as input, scaled by a factor *ds* and substracted from the latter vector $\vec{a}^0(r)$. In general form, $\vec{a}^{n+1}(r)$ calculates to

$$\vec{\alpha}^{n+1} = \vec{\alpha}^n - \left.\frac{\partial \Delta(\vec{\alpha})}{\partial \alpha_i}\right|_{\vec{\alpha}^n} ds \quad (12)$$

With this new vector the mean square deviation $\Delta(\vec{a}^{n+1}(r))$ was calculated again and compared to $\Delta(\vec{a}^n(r))$. If the new value was larger than the old one, the scaling factor *ds* was decreased and this step repeated until an increase of $\Delta(\vec{a}^{n+1}(r))$ was obtained. Then the whole process was repeated until a minimum in the mean square deviation $\Delta(\vec{\alpha}(r))$ was reached. In practice the iteration was terminated when the absolute value of the gradient was smaller than a given treshold.

For samples separated by SEC or other fractionation methods a distributon vector $\vec{a}(r)$ has to be calculated for every elution volume. For a well separated sample this vector - interpreted as N different points of a distribution function $\alpha(r)$ - shows a narrow distribution peak. If the sample still remains polydisperse after fractionation, a broader distribution is obtained, or, if two different populations are sufficient different in their size, two peaks for $\vec{\alpha}$ at one elution volume V. This effect can occur in particular on separating highly polydisperse samples by Field-Flow-Fractionation techniques. In this method very large particles are eluted by a different mechanism than small particles, such that small and large particles are eluted at the same elution volume.

Application to Model Structures

a) Test with simulated angular intensity distributions

To test the evaluation by Legendre polynomials, the technique was applied to the two well-known form factors of solid and hollow spheres. The form factor for a solid sphere is [5]

$$P(\vartheta) = \left(\frac{3(\sin qr - qr\cos qr)}{(qr)^3} \right)^2 \qquad (13)$$

and the form factor of a hollow sphere [5]

$$P(\vartheta) = \left(\frac{\sin qr}{qr} \right)^2 \qquad (14)$$

To simulate a measurement, the form factor was calculated for the 16 detector angles of the Dawn instrument with an aqueous solution (14.5° - 158.3°), as listed in [6], and a wavelength of $\lambda_0 = 632.8$ nm. The integration was performed as described above, approximating the value for 0° by linear extrapolation of the intensities at the first two angles. Figure 2 shows the input values for the Legendre expansion and the resulting function for spheres of several radii, Figure 3 shows a comparison of the calculated results for solid spheres and spherical shells.

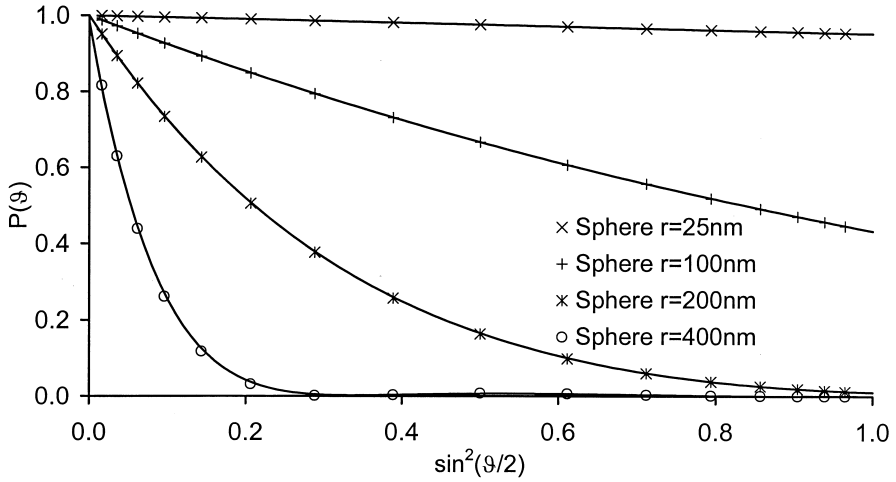

Figure 2: Legendre expansion for theoretical form factors of solid spheres. As inputs the values for a set of 16 angles were used, indicated by the symbols. The solid lines are the results of Legendre expansion.

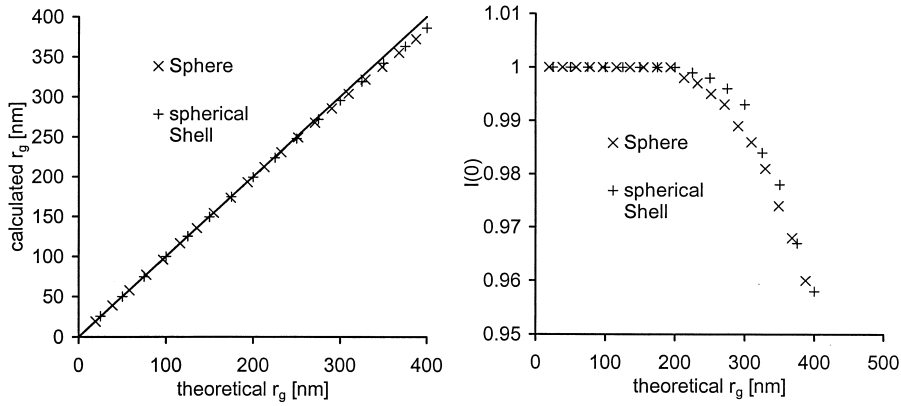

Figure 3: Comparison of the results for spheres and spherical shells. The left figure shows the results of the Legendre expansion vs. the theoretical radii of gyration. The deviations in the range 300-400nm are smaller than 5%. The right figure shows the calculated form factor for ϑ=0°

Excellent agreement was obtained up to radii of gyration of 200 nm. For larger radii the inaccuracy of determining $P(0)$ by the mentioned extrapolation is shown on the right side of figure 3. The deviation is less than 5%. However, no noise of the data was superimposed.

On the other hand this size range $r \geq 200$ nm is no longer in the range of the Debye-Gans-approximation. The method works satisfactorily in the range of the Debye-Gans-approximation and correct values for the radius of gyration and the molar mass can be obtained.

b) Influence of linear extrapolation on the initial data point

To determine the coefficients a_i with eq. (7), the integral has to evaluated over the range $\sin^2(\vartheta/2) \in [0..1]$. The integration can be performed numerically dividing the intervall in slices corresponding to the experimental angles, but for the first point $\sin^2(\vartheta/2)=0$ and for the last point $\sin^2(\vartheta/2)=1$ an approxiamtion is necesary. The choice of the first data point is important for a correct calculation. This problem was solved in the expansion formalism by linearisation of the first two known intensities towards zero angle. As shown, the agreement in the Debye-Gans-region for spherical particles is very good. In order to investigate the influence of the first point on the final results, the theoretical form factor of a solid sphere (r=300nm) was taken at the 16 angles from the Dawn instrument [6]. A data point at $\vartheta=0°$ was added and systematically varied from 0.5 to 1.5 (1.0 beeing the correct value). These 17 data points were now used as input for the integration and the radius of gyration r_g as well as the intercept $P(0)$ was calculated. The results are given in table 1 and compared to the theoretical values.

Table 1: Calculated r_g and $I(\vartheta=0)$ for a sphere with a radius r=300nm (r_g=232.4 nm) by variation of the intensity for the 0°-angle. The stopping criterion was chosen as explained above, the number of terms used are shown in the column #terms

I(0)	# Terms	R [nm]	Δr [%]	I(0)	ΔI [%]
0.5	3	194.8	-16.2	0.834	-16.6
0.6	3	195.4	-15.9	0.847	-15.3
0.7	3	196.1	-15.6	0.859	-14.1
0.8	4	215.6	-7.2	0.935	-6.5
0.9	4	217.5	-6.4	0.954	-4.6
1.0	7	232.4	0	1	0
1.1	18	393.8	69.45	1.129	12.9
1.2	18	467.3	101.1	1.243	24.3
1.3	18	520.6	124.0	1.358	35.8
1.4	18	561.6	141.7	1.472	47.2
1.5	18	594.5	155.8	1.586	58.6

If the first point is chosen smaller than the theoretical value of 1, the deviations in the results for r_g and $I(0)$ are smaller than the input deviations, but increase dramatically if the first data

point was chosen higher than the theoretical value. This behavior of the Legendre formalism is explainable by the number of terms used for the expansion. The stopping criterion is that three succeeding expansion coefficients should be smaller than a given value, or that one value would be smaller than zero. If the first data point is too small (and even smaller than the second), the formalism is stable, because a positive slope is avoided by the stopping criterion. If the first data point is too high, it will be fitted by higher terms in the Legendre expansion and the number of required Legendre polynomials increases rapidly. This effect is demonstrated in figure 4, where two calculated form factors with the first values set to $I(0)$=0.5, 1 and 1.5 are depicted. The cross symbols mark the 16 input values, the lines the calculated form factor $\tilde{P}(\sin^2 \vartheta/2)$ for the different first data points. Note that the formalism results a very high slope for the curve with $P(0)$=1.5 for small ϑ to fit this point, but that the error for the $P(0)$=0.5 curve is much smaller.

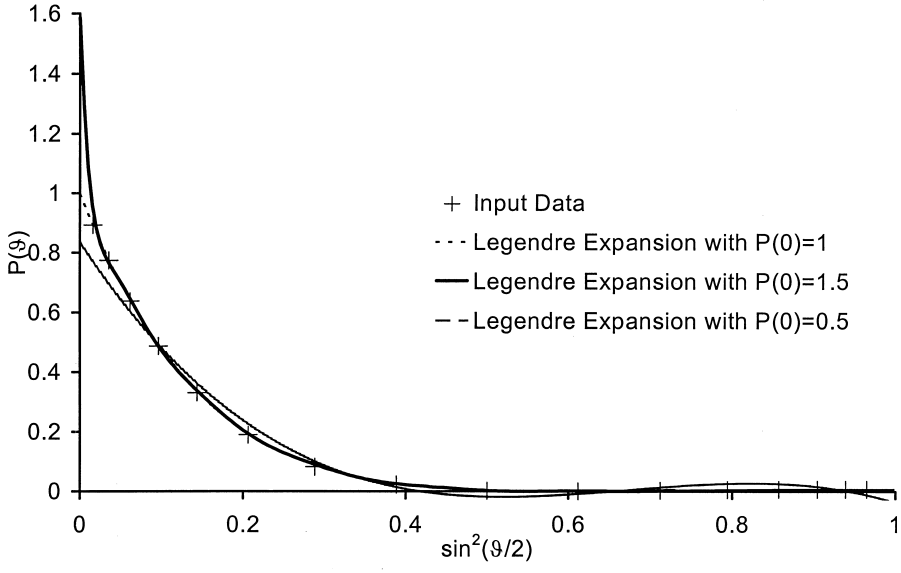

Figure 4: Calculation of $\tilde{P}(\sin^2 \vartheta/2)$ using different first values. The input was the theoretical form factor of a sphere r=300nm at 16 angles and a value of $P(0)$=0.5, 1, 1.5

Even if the first data point is by 50% too small, the calculated form factor has no positive slope at $\sin^2 \vartheta/2$=0.

The calculation for the form factor after linear extrapolation of the first data points yields R_g=230.4 nm, $I(0)$=0.9964. A linear extrapolation of the first known data points results

$I(0)$=0.989. The initial slope of theoretical form factors is always negative, a linearisation of the first data points and extrapolation to zero will therefore give allway a smaller number than that of $\tilde{P}(\sin^2 \vartheta/2 = 0)$. The formalism applied to the trunctation of the Legendre polynomials causes a stable range of evaluation.

4 Experimental Results

a) Latex particles

The mathematical concept was examined with measurements from PS-Latex Particles (Duke-Standards) of four different sizes. In Figure 5 the measured intensities, normalized by $I(0)$=1 (crosses) and the calculated form factors are shown.

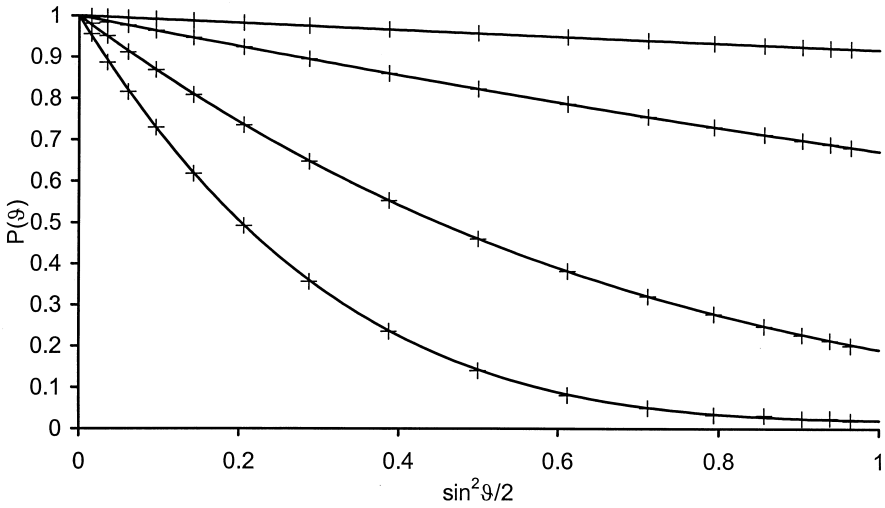

Figure 5: Measured intensities of Duke-PS-Standards (crosses) (r=25 nm, 52.2 nm, 102 nm and 152 nm) and calculated form factors plotted vs. $\sin^2(\vartheta/2)$.

Table. 2: Light Scattering measurements of Duke-Standards. The deviation of the theoretical size and the size determined by the evalutaion of the experimental data using Legendre-expansion is smaller than 3%

Theoretical		Experimental Results	
r_{Sphere}	$r_{gyration}$	$r_{gyration}$	Deviation
25 nm	19.4 nm	19.8 nm	2.1%
52.5 nm	40.7 nm	40.6 nm	-0.2%
102 nm	79.0 nm	78.7 nm	-0.4%
152 nm	117.7 nm	116.4 nm	-1.1%

In Table 2 the theoretical radii of gyration are compared with the measured ones. The observed deviations are smaller than 3%.

b) Results from Mistletoe extracts separated by asymmetric FFF (aFFF)

Mistletoe extracts, which are investigated in the laboratory of the Carl Gustav Carus-Institute, are known for cancer therapy since 70 years. These extracts are prepared by homogenization of mistletoe leaves and berries in a french-like press. A very complex colloidal system is obtained that contains vesicles from the cell membranes together with large polysaccharides and a number of low M_w compounds. The partially coagulated particles cover a molar mass range from a 10^5 to 10^{10} Da. Separation was performed by aFFF [7]. This system consists of a long, flat channel. At the bottom of the channel a membrane is installed on a porous support. The channel flow, which has a parabolic flow profile, is divided into two parts, the one exits at the channel output, the other forms a cross flow through the membrane. The movement of particles in the channel is influenced by three forces: one force drives the particles towards the exit by the channel flow, another towards the membrane by the cross flow and finally, the diffusion force drives them back into the channel. For small particles the force by the cross flow is weaker than the effect of diffusion. The particles move towards the middle of the channel and are eluted faster than large particles, which are pushed closer to the membrane by the cross flow and are in a region of lower channel flow. This elution mode is called the normal elution.

Very large particles are pressed onto the membrane, but they protrude into the channel and reach the region of high channel flow (steric elution). Furthermore, they can be driven further into the channel due to lift forces (hyperlayer elution). For these particles the elution mode is inverted, at first the large particles are eluted followed by the smaller ones. For colloidal polydisperse systems, covering a large range in sizes, these modes may superimpose, depending on the flow rates. At the beginning of the elution the largest and the smallest particles are eluted simultaneously. With increasing elution time, the particles eluted by the normal mode increase in size as the elution volume increases. On the other hand the particles eluted by the steric/hyperlayer mode decrease in size. Both branches meet at the inversion point, where both sizes are equal. This inversion point can be shifted by varyiing the flow rates of the channel- and the cross-flow.

To study this behavior, we applied the form factor analysis to different flow rates. The results are shown in the graphs of Figure 6 and Figure 7.

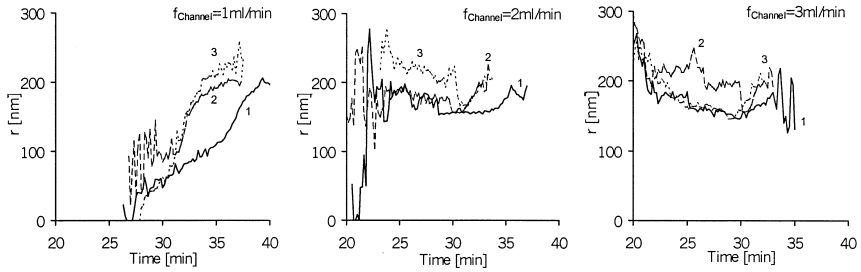

Figure 6: Calculated radii of gyration vs. Elution time of Mistletoe extracts for various flow parameters of the aFFFF. The numbers plotted at the curves indicate the start flow of the cross flow in ml/min, which was reduced within 15 minutes to zero. The left diagramm shows normal elution, the middle one superimpose of normal and steric elution and the right one steric/hyperlayer elution.

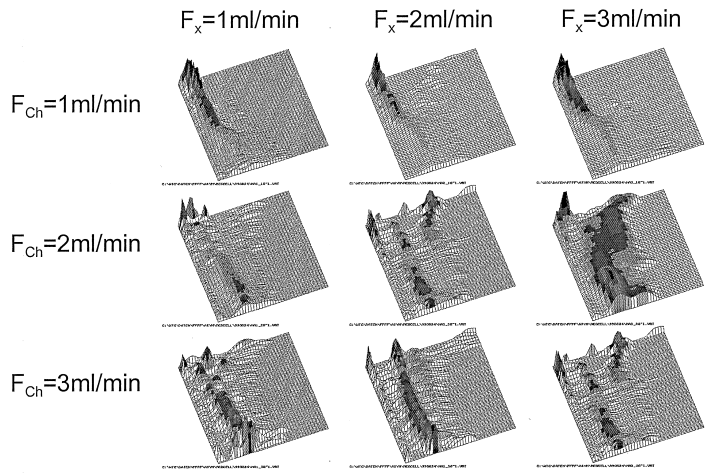

Figure 7: Results of the form factor analysis for various flow rates of the measurement shown in Figure 6. The x-axis shows the elution volume, the y-axis the radius of the hollow spheres used for the fit and the z-axis the distribution function $\alpha(V,r)$. F_{Ch} means channel flow and F_x cross flow

The channel flow was varied from 1ml/min to 3 ml/min, the cross flow was a function of time, starting at 1··3 ml/min and reduced to zero within 15 minutes. For the channel flow of 1ml/min, the variation of the cross flow has only a small effect. The plot of the r_g (Figur. 6) shows a normal elution mode from small to large particles. Increasing the channel flow to 2 ml/min, the r_g-plot shows nearly a average constant size of the particles on elution, with the exception of the beginning of the elution, where the concentration is very small. The form

factor analysis shows with increasing cross flow the hyperlayer/steric branch and the polydispersity of the particles becomes obvious in such separation. For the channel flow of 3 ml/min, the R_g-plot shows a decreasing radius, which can be interpreted as steric/hyperlayer elution. The form factor analysis confirms this interpretation. A problem is the dilution of the sample in the channel, which increases with increasing channel flow, but the form factor analysis still allows observation of the separation character.

Conclusions

In this paper a method was suggested and examined to calculate an analytical function for the form factor from static light scattering experiment using Legendre polynomials. This method gave correct radii of gyration and correct molar masses within the Debye-Gans-region.

Furthermore, a method was presented to deconvolute form factors from an ensemble of hollow spheres. This procedure allows to draw information about the polydisperity of the samples. An example was shown with superimposing elution modes for aFFFF separations of highly polydisperse mistletoe extracts.

References

[1] M. Kerker; The Scattering of Light, Academic Press; New york; 1969
[2] B.H. Zimm; J. Chem. Phys. 16(1948)1093ff
[3] A. Guinier; Ann. Phys. 12(1939)161
[4] I.N. Bronstein, K.A. Sjemendjajew; Taschenbuch der Mathematik; Verlag Harry Deutsch, Thun 1987
[5] W. Burchard; Light Scattering Techniques in: Applied Fibre Science, (Ed. F. Happey) Academic Press London 1978, Chapter 120
[6] Dawn-F Instruction Manual; Wyatt Technology Corporation; Santa Barbara 1991
[7] J.C. Giddings; Science 260(1993)1456

Acknowledgment
It is a pleasure for me to thank Prof. Dr. W. Burchard, University of Freiburg, Institute of Macromolecular Chemistry for many helpful discussions and hints.